Interphase Design for Lithium-Metal Anodes

Wang, Qidi; Zhao, Chenglong; Wang, Shuwei; Ombrini, Pierfrancesco; Ganapathy, Swapna; Eustace, Stephen; Armand, Michel; Aurbach, Doron; Wagemaker, Marnix; More Authors

DOI
10.1021/jacs.4c15759

Publication date
2025

Document Version
Final published version

Published in
Journal of the American Chemical Society

JACS
JOURNAL OF THE AMERICAN CHEMICAL SOCIETY
pubs.acs.org/JACS
Article

Interphase Design for Lithium-Metal Anodes

Qidi Wang,*[,∇] Chenglong Zhao,[∇] Shuwei Wang,[∇] Jianlin Wang, Fangting Wu, Pierfrancesco Ombrini, Swapna Ganapathy, Stephen Eustace, Xuedong Bai, Baohua Li, Michel Armand,* Doron Aurbach,* and Marnix Wagemaker*

Cite This: J. Am. Chem. Soc. 2025, 147, 9365−9377

Read Online

ACCESS | Metrics & More | Article Recommendations | Supporting Information

ABSTRACT: Electrode−electrolyte interphases are critical determinants of the reversibility and longevity of lithium (Li)-metal batteries (LMBs). However, upon cycling, the inherently delicate interphases, formed from electrolyte decomposition, become vulnerable to chemomechanical degradation and corrosion, resulting in rapid capacity loss and thus short battery life. Here, we present a comprehensive analysis of the complex interplay between the thermodynamic and kinetic properties of interphases on Li-metal anodes, providing insights into interphase design to address these challenges. Direct measurements of ion-transport kinetics across various electrolyte chemistries reveal that interphases with high Li-ion mobility are essential for achieving dense Li deposits. Conversely, sluggish ion transport generates high-surface-area Li deposits that induce Li random stripping and the accumulation of isolated Li deposits. Surprisingly, interphases that support long cycle life do not necessarily require the formation of dense Li deposits but must avoid possible electrochemical/chemical reactions between the Li-metal deposits and electrolytes' components. By that, in some specific electrolyte systems, isolated Li deposits can recover and electrically rejoin the active Li anodes' mass. These findings challenge conventional understanding and establish new principles for designing durable LMBs, demonstrating that even with commercial carbonate-based electrolytes, $LiNi_{0.8}Co_{0.1}Mn_{0.1}O_2$||Cu cells can achieve high reversibility.

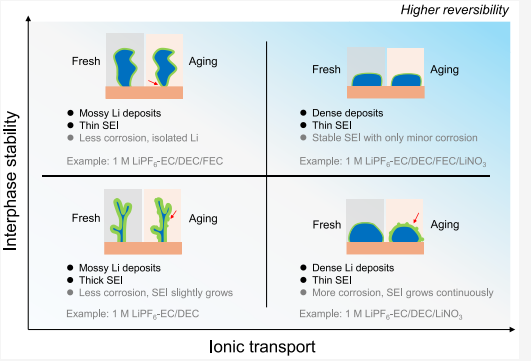

INTRODUCTION

Pursuing higher energy densities in batteries has led to intensive efforts in developing rechargeable batteries with lithium (Li)-metal anodes, which offer the highest theoretical specific capacity and the lowest electrochemical redox potential.[1−4] However, the challenges lie in achieving high reversibility and long cycle-life, owing to uncontrolled dendritic growth of Li deposits, inducing the formation of dead Li metal, and hence degradation of the Li anodes.[3,5] One important approach to address these issues is modification of the electrolyte systems, which has demonstrated important advances in the performance of such batteries.[6−8] Commercial Li-ion batteries (LIBs) primarily employ carbonate-based electrolytes owing to their apparent electrochemical stability in Li-ion cells. This stability is reached thanks to their intrinsic high anodic stability (>4.3 V vs Li) and formation of surface films upon their reduction at potentials below 1.5 V vs Li, which precipitate on the lithiated graphite anodes as reliable solid-electrolyte interphases (SEIs) that passivate and protect them.[8] There are clear advantages in the use of alkyl carbonate-based solutions in rechargeable Li batteries in terms of cost-effectiveness, versatility in possibly manipulating the interfacial surface chemistry in the cells, and acceptable safety features. However, electrolyte solutions based on carbonate solvents show limitations when applied to Li-metal anodes, as their detrimental interfacial reactions result in low coulombic efficiency (CE).[9−11] Extensive efforts have been dedicated to different electrolytes and interfacial concepts over the years;[6,12−19] however, the disparity between the current performance of these electrolyte systems for Li-metal anodes and the demands relevant for rechargeable batteries impedes the practical application of carbonate-based electrolyte solutions in such batteries. In studies exploring advanced electrolytes, conventional carbonate-based electrolytes are typically used as a reference for comparison,[13,14,18−21] always being outperformed by the newly developed electrolytes. Much less effort has been devoted to comprehensively understanding their failure mechanisms and identifying opportunities to improve the understanding of interphases, which could significantly promote the development of advanced electrolytes for high-energy rechargeable batteries based on Li-metal anodes.

Received: November 18, 2024
Revised: February 21, 2025
Accepted: February 21, 2025
Published: March 7, 2025

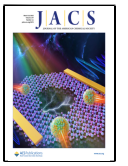

https://doi.org/10.1021/jacs.4c15759
J. Am. Chem. Soc. 2025, 147, 9365−9377

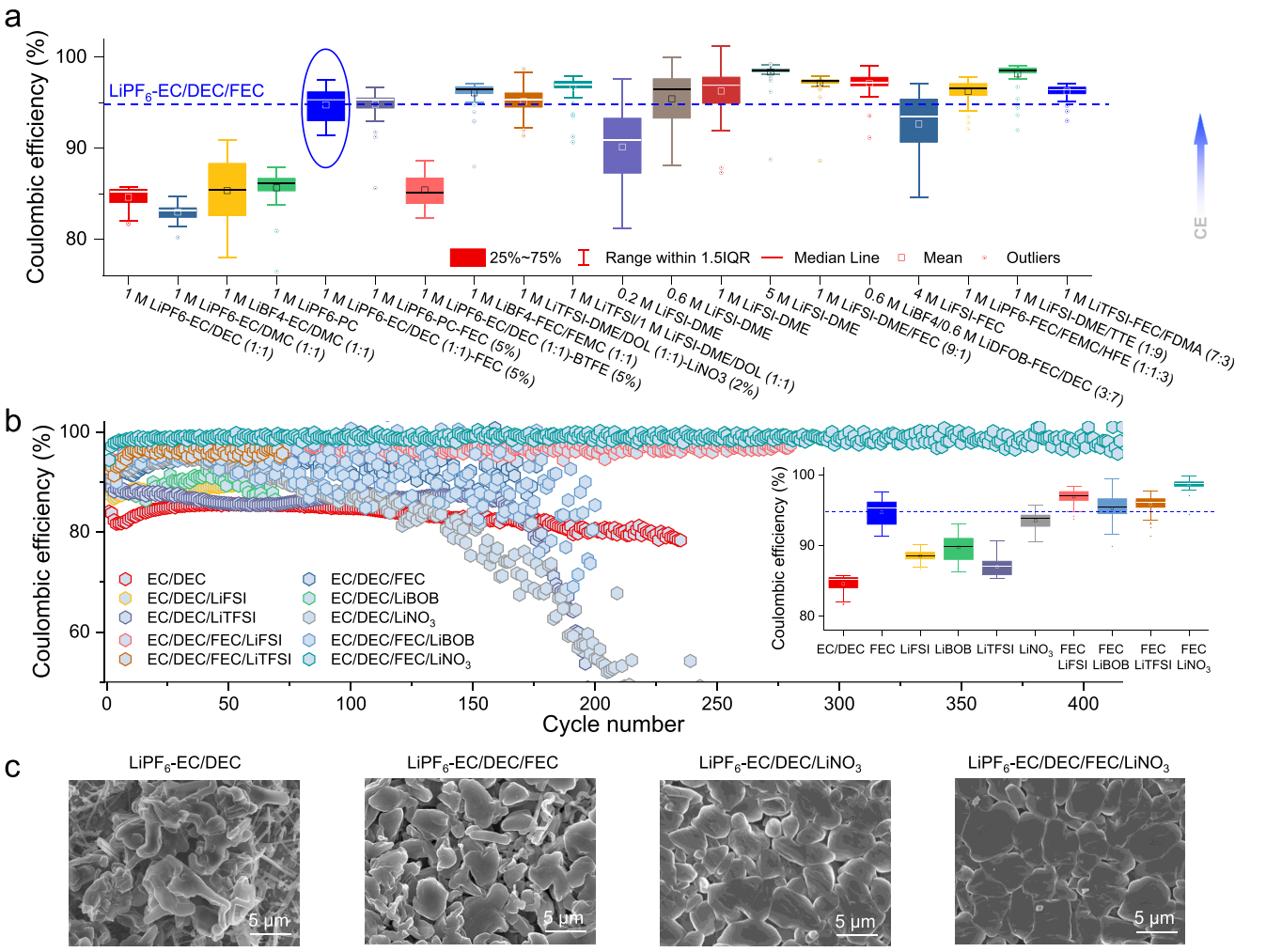

Figure 1. Electrochemical cycling and the Li-metal microstructure. (a) Electrochemical cycling of 20 kinds of representative electrolytes, prepared and cycled under the same conditions. The CE of the $LiPF_6$-EC/DEC/FEC electrolyte is indicated as a reference (blue dotted line). The center line of each box plot represents the median; lower and upper box limits represent the 25 and 75% quantiles, respectively; whiskers extend to box limit ±1.5 × IQR (interquartile range); outlying points are plotted individually. (b) Continuous Li plating/stripping CEs and statistics in $LiPF_6$ carbonate electrolytes with 0.1 M salt additives and 5% FEC (in volume). The statistical analysis is based on the first 60 cycles. (c) SEM images of Li-metal plating at 1.0 mA cm^{-2} for 1 h after ten cycles in different electrolytes as marked.

Aiming at understanding the interphase properties and developing advanced electrolytes for rechargeable Li batteries with Li-metal anodes, we conducted a comprehensive comparison of representative electrolytes, prepared and evaluated under the same conditions (Figures 1a and S1, and Table S1). Figure 1a shows that conventional carbonate-based electrolytes exhibit an average CE below ∼85%. Introducing the widely used fluoroethylene carbonate (FEC) additive, known to induce F-rich SEI species, the CE increases to approximately 90%; however, it is still far from the practical demands.[22−26] Ether-based electrolytes are more stable against reduction, resulting in a higher CE, especially by employing a high salt concentration (e.g., 5 M LiFSI of ∼99%) inducing a salt-derived SEI.[6,12,27] A similar effect is observed for locally concentrated electrolytes[6,18] by using a large amount of highly fluorinated diluting solvents. Additionally, highly fluorinated electrolytes, containing a substantial number of fluorinated cosolvents with a low donor number (DN) (see Table S2), contribute to weaker solvation interactions, facilitating a salt-derived and F-rich SEI.[15−17] These electrolytes show higher CEs, around 99%, suggesting that tuning the electrolyte formulations to form a salt-derived interphase is a key factor in improving the reversibility of Li-metal anodes. The study presented herein systematically examined the impact of SEI properties on the Li-metal plating/stripping behavior. By establishing correlations between the Li-ion transport properties across the SEI and their stability, we aim to develop a more comprehensive understanding and unleash the potential of practical electrolyte chemistries for Li-metal batteries (LMBs), with an emphasis on typical alkyl carbonate solvents and commercial Li salts in this context.

The starting point is a survey on the influence of several different Li salt additives, including LiTFSI, LiFSI, LiBOB, and $LiNO_3$ (the latter widely used in ether electrolytes, forming surface films rich in Li−N/O, which act as favorite SEI components[28]) to commercial 1 M $LiPF_6$-EC/DEC (baseline system) and 1 M $LiPF_6$-EC/DEC/FEC electrolytes (the reference system). These salts, commonly used in various types of Li batteries, were chosen for their relatively high reduction potentials (Figure S2 and Table S3), which allow them to actively participate in SEI formation, even when paired with highly reactive solvents. $LiNO_3$ is poorly soluble in

https://doi.org/10.1021/jacs.4c15759
J. Am. Chem. Soc. 2025, 147, 9365−9377

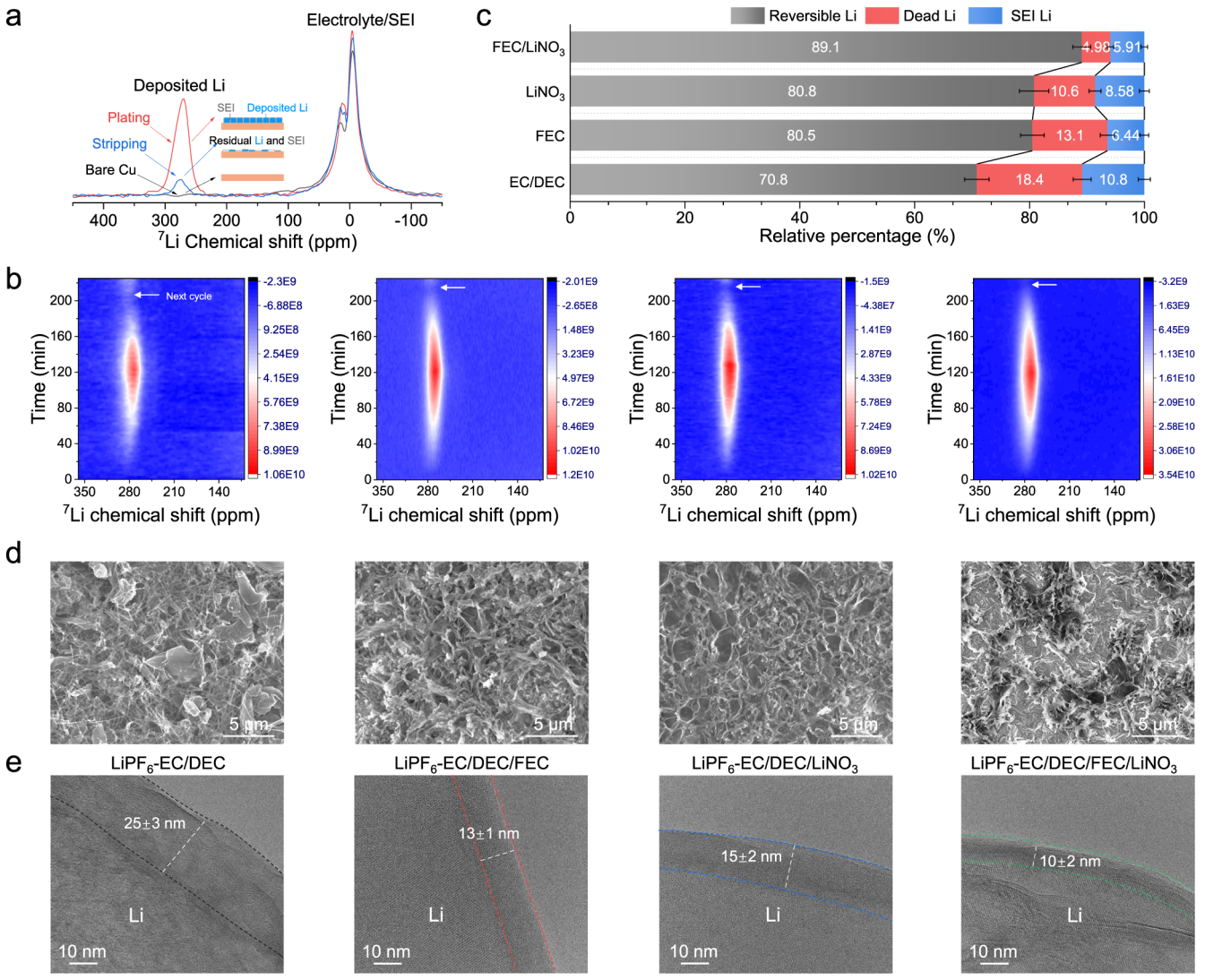

Figure 2. Operando ^{7}Li NMR for Li species quantification and microstructure. (a) Schematic illustration of the Li species resonance evolution upon (dis)charging the anode-free Cu||LiFePO$_4$ cells.[54] The Li-metal resonance (~270 ppm) represents the Li deposits on the current collector that are formed during charging and are removed during discharging. (b) Operando ^{7}Li NMR measurements upon charging/discharging in different electrolytes at a current density of 0.5 mA cm^{-2} for 2 h. The arrow indicates the end of this cycle. (c) Quantification of the Li species during cycling, Li species in SEI (blue bars), reversible Li metal (gray bars), and dead Li metal (red bars), derived from the Li-metal integrated intensity ratio and the electrochemical CE values. Error bars were calculated after the experiments were repeated three times. (d) SEM images of Li morphology after ten cycles in various electrolytes as indicated, ending with Li stripping to 1.0 V, showing the microstructure of the SEI and the dead Li-metal residues. (e) Microstructure of deposited Li metal and the SEI phase from cryo-TEM images. Error bars were calculated by measuring the SEI thickness in different regions.

carbonates, for which we developed a two-step approach that enhances the solubility of LiNO$_3$ in carbonate solvents (see Methods and Figure S3). As shown in Figure 1b, the small amount of additional salt (0.1 M) demonstrates an improvement in the CEs of the baseline 1.0 M LiPF$_6$-EC/DEC electrolyte to around 90% but shows inferior performance compared to the FEC additive. Unexpectedly, when the individual salt additives are used in combination with FEC, all CEs are significantly enhanced, where LiNO$_3$ with FEC results in the highest CE, exceeding 99%, suggesting this to be a promising route to improve carbonate electrolytes for LMBs. To understand the underlying mechanism of the observation, we perform a comprehensive study on the interphase properties (e.g., morphology, chemistry/structure, and Li-ion kinetics) and its correlation with the evolution of the Li-metal deposits upon cycling and aging. Four possible scenarios were studied: no additive, FEC as a single additive, LiNO$_3$ as a single additive, and both FEC and LiNO$_3$ as additives in the 1.0 M LiPF$_6$-EC/DEC baseline electrolyte. The results revealed that each specific SEI property induced by the electrolyte chemistry has advantages and disadvantages in both cycling efficiency and long-term stability. Systematic characterizations of operando/in situ and ex situ spectroscopy and imaging technologies, as well as various electrochemical test protocols, allowed us to unravel the complex correlation between Li-ion transport across the SEI and the stability of the resulting interphase, providing valuable insights for interphase design toward high-performance LMBs.

RESULTS AND DISCUSSION

Electrochemical Cycling and Li-Metal Deposition Morphology. First, we investigated the solvation structure

https://doi.org/10.1021/jacs.4c15759
J. Am. Chem. Soc. 2025, 147, 9365−9377

of the 1.0 M $LiPF_6$-EC/DEC baseline electrolyte with no additives, then with 5% FEC, with 0.1 M $LiNO_3$, and with the combination of both additives. ^{7}Li nuclear magnetic resonance (NMR) spectroscopy showed that the two additives have opposite impacts on the Li-ion environment, where FEC results in an upfield shift to −0.38 ppm and $LiNO_3$ results in a downfield shift to −0.32 ppm, compared to the baseline electrolyte located around −0.36 ppm (Figure S3). The variation in solvation strength is subtle, in line with the Raman spectra (Figure S4), which suggest that a small amount of additive does not significantly alter the solvation sheath of Li ions compared to the baseline electrolyte, consistent with previous reports.[20,29−32] However, the different reduction peaks at around 1.0−1.5 V observed in the cyclic voltammetry (CV) measurements upon adding FEC and/or $LiNO_3$ indicate that the additives impact the interphase formation (Figures S5 and S6), which offers an opportunity to explore the influence of the consequent interphase properties and how they correlate to the reversibility of Li deposition/dissolution processes upon cycling.

Compared to the baseline electrolyte, improved Li-metal plating/stripping performance was achieved with the additives upon continuous cycling of Li||Cu cells (Figures 1b, S7, and S8). During the initial ∼20 cycles, the use of a single $LiNO_3$ additive resulted in a higher CE and a lower overpotential, as compared to FEC. However, it suffered from rapid degradation during subsequent cycles. In contrast, the combination of both additives exhibited a higher CE (over 99%) and more stable cycling over 400 cycles, which is further supported by stable cycling for more than 4000 h in symmetric Li||Li cells (Figures S9 and S10). The morphology of the deposited Li metal was investigated by scanning electron microscopy (SEM) (Figures 1c, S11, and S12). The use of FEC as an additive increased the deposit size while still exhibiting porous and whisker-like structures. By comparison, the electrolytes with the $LiNO_3$ additive tend to have larger deposited particles and are additionally more compact, indicating that larger Li-metal deposits as such do not necessarily correlate to a higher CE, unlike what is commonly assumed. This is difficult to explain based on current understanding[28,31−35] and provides additional motivation for the present systematic study.

Quantification of Li-Deposited Species. To study the evolution of different Li-deposited species and the origin of the reversibility of cells, operando ^{7}Li solid-state NMR measurements were performed, presenting a noninvasive methodology for this analysis (Figure 2a).[36,37] Due to the Knight shift of deposited Li metal (240−290 ppm), it can be distinguished from the diamagnetic Li-ion species in the SEI/electrolyte (∼0 ppm), and their amount can be quantified.[36] As shown in Figures 2b and S13, upon charging Cu||$LiFePO_4$ cells, Li metal starts plating on the Cu current collector; thus, the Li-metal resonance (∼270 ppm) grows, which subsequently decreases upon stripping. Based on NMR spectra and the corresponding CE values of Li deposition measured electrochemically, the quantity of reversible Li metal, dead Li metal, and Li ions in SEI species can be calculated (see Methods). The percentage of reversible Li metal is proportional to the initial CE values (Figure 2c), showing the lowest value for the baseline electrolyte system used in this study and the highest value for the combination of FEC and $LiNO_3$ additives. The use of single-additive electrolytes resulted in a similar amount of reversible Li metal; however, the origin of the Li losses is different. Electrolyte with FEC induces more dead Li formation, while the presence of $LiNO_3$ generates more Li-containing species in the SEI. This is consistent with the SEM images of the Cu current collector after stripping. Figure 2d indicates massive whisker-like Li residues and some large deposits left on the anodes in experiments with the baseline electrolyte after stripping. For the electrolyte with FEC as a single additive, fewer residues were observed, though small Li deposits were left unconnected after stripping. In contrast, adding $LiNO_3$ to these electrolytes, with or without FEC, prevented the formation of observable isolated Li deposits. Combined with FEC (i.e., using $LiPF_6$−EC/DEC/FEC/$LiNO_3$ electrolyte solutions), it further reduced the amount of disconnected Li residues remaining on the anodes' surfaces after stripping.

The microstructure of the Li deposits and the surface films formed on them were further investigated by stabilizing their chemical and morphological states through cryogenic conditions using cryo-transmission electron microscopy (cryo-TEM). As shown in the low-magnification images (Figure S14), the whisker-like Li deposits formed in the baseline electrolyte are covered by a relatively thick and uneven SEI. Adding FEC as an additive affected the morphology of the Li deposits: the diameter of the whiskers increased, while more kinks appeared, which prevented the formation of larger bulk Li-metal deposits. Conversely, in electrolytes with $LiNO_3$, bulk-like Li-metal deposits appeared, having a larger average diameter and a smoother surface. These variations in the Li deposits' microstructure are related to the different properties of their protecting surface films. The high-resolution cryo-TEM images in Figure 2e show a thick SEI of 25 ± 3 nm formed on the Li deposits in the baseline electrolyte, which decreases upon adding $LiNO_3$. The SEI formed on the Li deposits in both baseline and $LiNO_3$-containing electrolytes is dominated by amorphous components, in which a small number of crystalline domains are randomly dispersed, forming a mosaic-type SEI structure (Figure S15). When the electrolytes used contained FEC, the SEIs formed on the Li deposits were also thinner compared to those formed in the baseline electrolyte. They included more crystalline/inorganic components, especially in their outer regions (Figure S16), compared to those formed on Li deposits in the baseline and $LiNO_3$-containing electrolytes, indicating a multilayer SEI structure. The use of both FEC and $LiNO_3$ in electrolytes resulted in the formation of a thinner SEI layer of 10 ± 2 nm with a multilayer structure, in line with the lowest amount of Li species observed within the SEI by the operando NMR measurements. Interestingly, it seems that the thicker SEI formed when only $LiNO_3$ is contained as an additive promotes large bulk Li-metal growth, whereas the thinner SEI formed in electrolytes containing FEC seems to result in whisker-like deposits. This suggests that the SEI thickness alone does not dictate the Li-metal deposition behavior.

Interphase Li-Ion Transport. One of the most crucial but also least quantified and understood properties of the SEI formed on Li metal anodes is their Li-ion mobility, which is very challenging to measure under realistic conditions.[38,39] Here, we make use of chemical exchange saturation transfer (CEST)-NMR measurements to quantify the Li-ion transport across the SEI toward Li metal, exploring its potential impacts on the Li-metal anodes. It is based on the exchange between a detectable large pool and an "invisible" small pool of interest to identify the exchange within different chemical environments (Figure 3a).[40−42] In LMBs, Li ions in the SEI can be

https://doi.org/10.1021/jacs.4c15759
J. Am. Chem. Soc. 2025, 147, 9365−9377

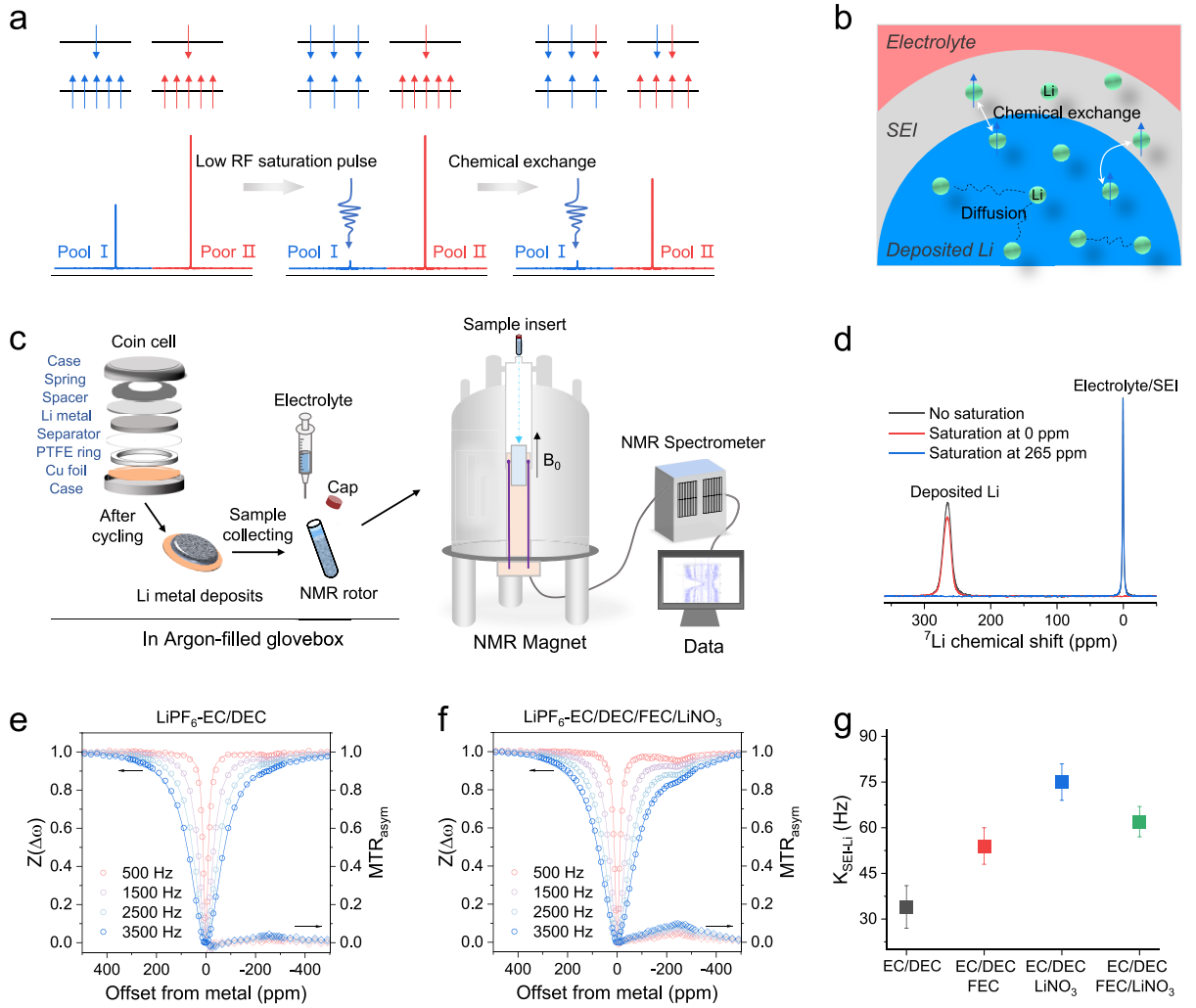

Figure 3. Qualitative analysis of Li-ion transport across interphases. (a) Principles of the CEST approach. For a two-pool system that has the same species at a specific RF (i.e., ^{7}Li in the metal and in the SEI), one pool is invisible by NMR detection, i.e., low-concentration "pool I", and the other is directly NMR detectable, i.e., large "pool II". Typically, a soft saturation pulse is applied on pool I, and the signal in pool II will decrease due to the chemical exchange with pool I, where accounting for the change of pool II signal allows probing the properties of pool I in higher sensitivity. (b) Schematic diagram of the CEST effect on "deposited Li metal and SEI" in a two-pool system. Through the application of a soft saturation pulse on the SEI resonance (~0 ppm, pool I), Li exchange occurs between the SEI and the deposited Li on which the SEI was formed (~265 ppm, Pool II), resulting in a decrease in the deposited Li signal. (c) Schematic process of samples' preparation for CEST measurements. Cu foils were used as the working electrodes for Li-metal plating in coin cell setups with a PTFE ring as the separation layer. The cells were cycled using the procedure in Figure S17, and then, the Li-metal deposits were transferred into an NMR rotor in an Ar-filled glovebox and immersed in the corresponding electrolytes to keep the SEI and plated Li metal in their native environment. (d) ^{7}Li NMR spectra with or without a saturation pulse of 3500 Hz. (e, f) Z-spectra obtained from Li-metal deposits as a function of different saturation frequencies and the magnetization transfer ratio asymmetry (MTR_{asym}) analysis of Z-spectra. $\Delta\omega$ is the applied frequency away from the Li-metal peak. (g) Exchange rates via fitting the Z-spectra from the two-pool BMC equation.

exchanged with the Li-metal anode on which it is laid, forming a two-pool system, as illustrated in Figure 3b. With this powerful NMR spectroscopic method, the Li-ion exchange between Li metal and the SEI can be directly probed in its native state,[40,43] using the sample preparation protocol shown in Figure 3c, as well as by note 1, Figures S17 and S18, and the Methods section. ^{7}Li nutation experiments reveal that entire Li deposits can be efficiently excited and detected by radio frequency (RF) pulses (Figure S19), and thus, CEST can quantitatively capture the Li-ion exchange rate between Li metal and the SEI formed on it (Figures 3d and S20).

Using CEST, the difference in interphases' Li-ion kinetics can be evaluated among different Li-electrolyte systems. The evolution of the Li-metal integral intensity as a function of saturation offset, which is obtained by the CEST experiments for a series of saturation frequencies ($\Delta\omega$), resulted in the Z-spectra plotted in Figures S21 and S22. Z-spectra with various RF saturation amplitudes (B_1 fields) from 500 to 3500 Hz (Figures 3e,f and S23) indicated that the CEST effect increased with the saturation amplitude B_1, corresponding to the increased MTR_{asym} signal that rules out interference with direct saturation.[44] The CEST effect is observed when the saturation pulse is centered around the resonance of the SEI resonance (~0 ppm), and this is accompanied by a change in the Li-metal signal intensity. From a cursory examination of the Z-spectra depicted in Figure 3e,f, the results suggest that the SEI formed in the baseline electrolyte reflects the lowest CEST effect, while the SEI formed in electrolytes containing

https://doi.org/10.1021/jacs.4c15759
J. Am. Chem. Soc. 2025, 147, 9365−9377

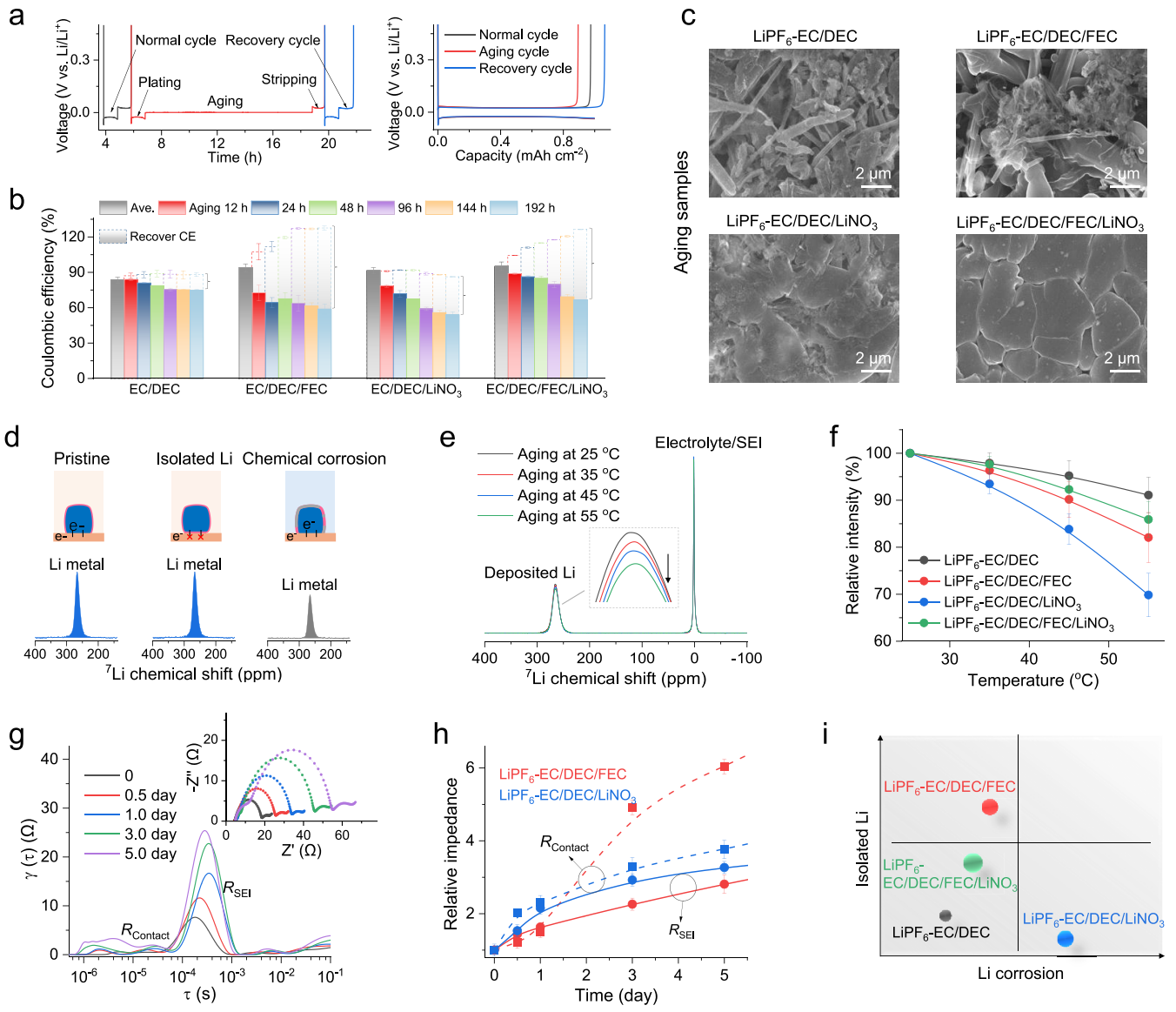

Figure 4. Quantitative analysis of interphase stability. (a) Illustration of the intermittent cycling protocol. Normal cycle: Li||Cu cells undergo three continuous cycles at a current density of 1.0 mA cm^{-2} for 1 h (1.0 mA h cm^{-2}). Aging cycle: Li metal is plated at a current density of 1.0 mA cm^{-2} for 1 h and then aged for different periods and then stripped at 1.0 mA cm^{-2} to the cutoff voltage of 1.0 V. Recovery cycle: following the aging cycle, a continuous Li plating−stripping process is conducted using the same current density as before. During the aging step, chemical corrosion occurs at the root or curved regions of whisker-like Li-metal deposits due to side reactions with the electrolyte solution species, leading to the formation of dead Li metal. However, during the recovery cycle, newly deposited Li metal reconnects with the isolated Li metal formed during aging, creating a conductive pathway for electron transport. This reconnection forms a conductive path for electron transport, allowing the previously dead Li to be recovered and reactivated for further cycling, contributing to a recovery rate exceeding 100%. (b) CE statistics of electrolytes during intermittent cycling. Brackets show the CE difference between the recovery cycle and the aging cycle. (c) SEM images of deposited Li after aging for 120 h. Cells were cycled at 1.0 mA cm^{-2} for 1 h after ten cycles and then plated for 1 h. (d) Schematic of quantification for the Li-metal deposits during aging using the in situ ^{7}Li NMR. Chemical corrosion occurs due to the reaction between Li deposits/SEI and electrolyte, forming dead Li or new Li-containing species, which can be effectively differentiated by the ^{7}Li NMR chemical shifts. The isolated Li metal should have a similar intensity as that of the pristine Li metal, while the electrochemical/chemical corrosion decreases the Li-metal signal. (e) In situ ^{7}Li NMR spectra acquired after aging at different temperatures for cells with the baseline electrolyte. It shows a decrease in the deposited Li-metal signal. (f) Relative intensity evaluation of the deposited Li metal using cells containing different electrolytes at increasing temperatures. (g) DRT analysis of the cells as a function of aging time. The inset shows the corresponding EIS data of these cells. (h) Interphase impedance (R_{SEI}) and contact impedance ($R_{Contact}$) of deposited Li metal relative to the initial impedance value (without aging) as a function of aging time of cells containing different electrolytes. (i) Illustrating the formation of isolated Li and chemically corroded Li for cells containing the different electrolytes after aging.

FEC and $LiNO_3$ significantly increases this effect (Figure S24). To quantify the exchange rate, the *Z*-spectra acquired with multiple B_1 fields were fit simultaneously using solutions to the two-pool Bloch−McConnell (BMC) differential equation (see Methods for details),[45−47] with the fitting parameters and boundaries listed in Table S4. As shown in Figure 3g, the exchange rates for the interphases formed in the four electrolytes are significantly different, where the additives induce higher Li-ion exchange rates and thus larger Li-ion diffusivities compared to the SEI formed in the baseline

https://doi.org/10.1021/jacs.4c15759
J. Am. Chem. Soc. 2025, 147, 9365−9377

electrolyte (Table S5). The SEI that forms upon adding $LiNO_3$ alone results in the highest exchange rates across the metal−SEI interface, even though the relevant SEI is thicker than that formed in the FEC-containing electrolytes, leading to the large Li-metal deposits observed. In contrast, a lower exchange rate through the SEI formed in the FEC-containing electrolytes appears to be responsible for the more whisker-like Li deposition.

Interphases Stability. In addition to continuous electrochemical cycling, where the stability of LMBs is associated with accumulated Li losses, including the formation of dead Li deposits and SEI species, chemical corrosion can also lead to SEI dissolution and active Li-metal loss due to the less passivated Li-metal surfaces.[48] This aspect is important for continuous cycling and particularly relevant during periods of batteries held on (storage at rest, no activity), which occur in real-life applications but receive relatively little attention in current research.[49,50] To address this issue, we employed intermittent electrochemical test protocols that include calendar aging steps (Figure 4a) to study the interphase degradation and the consequent electrolyte consumption through side reactions with the electrodes. Figure 4b illustrates that during intermittent cycling of Li||Cu cells, the use of the baseline electrolyte leads to smaller CE fluctuations between aging and recovery cycles (Figures 4b and S25−S27). However, it has a lower average CE of around 83%. In comparison, both FEC-added electrolytes show larger CE fluctuations but higher average CE values. Cells with the electrolyte containing only the $LiNO_3$ additive exhibit initially a relatively higher CE (∼93.6%); however, it decreases with increasing aging time. The CE value statistics indicate that these electrolytes experience different capacity loss mechanisms upon aging. (1) FEC-added electrolytes induce more dead Li deposits during each aging step, as evidenced by recovery with CE values exceeding 100% during subsequent recovery cycles. (2) The single $LiNO_3$-added electrolyte did not exhibit any increase in their CE values during the recovery cycles after intermittent aging steps but rather a decreased CE with increasing aging time, indicating a higher susceptibility to chemical corrosion and the formation of irreversible Li-containing products. (3) The smaller CE fluctuation observed with cells containing the baseline electrolyte suggests that their electrodes' interfaces undergo fewer chemical reactions and form less dead Li at aging.

To clarify this, the corresponding morphologies after aging were characterized. Figure 4c shows extensive side-reaction products on deposited Li metal in the $LiNO_3$-containing electrolyte, compared to the morphology of deposited Li metal in the baseline electrolyte (Figure 1c), indicating harsh corrosion during aging. Indeed, Li deposits aged for several hours in the baseline electrolyte exhibited less severe chemical corrosion compared to those formed and aged in the $LiNO_3$-containing solution (Figures 4c and S28). Interestingly, while Li deposits aged in electrolytes containing either FEC or $LiNO_3$ (as single additives) show a porous/rough morphology, the Li deposits aged in electrolytes containing both FEC and $LiNO_3$ displayed smooth and clean surfaces. These observations provide evidence of varying degrees of chemical corrosion, depending on the electrolyte compositions that induce unique surface chemistries. Electrochemical statistics also support this, indicating that the chemical stability of the interphase plays a crucial role in determining the performance of batteries, which include active interfaces like LMBs and LIBs. Specifically, the properties of the interphases on the electrodes affect dead Li-metal formation, and/or they determine the number of Li-containing species formed on the electrodes through the reactions between the electrolyte and Li metal deposits, as illustrated in Figure 4d. However, a full understanding of these complex correlations remains challenging.

Then, utilizing the capability of NMR spectroscopy to quantify various Li species, we employed in situ measurements to monitor Li-metal deposition during aging, which offers further insights into the degradation mechanism of Li anodes (Figure 4d and see Methods). A temperature gradient program was applied at each temperature to amplify the interphase degradation upon aging. The Li-metal peak intensity decreases at higher temperatures and longer aging times in all electrolytes, indicating chemical corrosion of Li metal (Figures 4e and S29). Corrosion rates in different electrolytes are shown in Figure 4f. The baseline electrolyte exhibits the least Li-metal loss, suggested to be the consequence of the thicker interphase layer formed in it (Figure 2e) dominated by the higher carbon content detected by X-ray photoelectron spectroscopy (XPS) (Figures S30−S33). This confines the Li-metal deposits within the SEI during cycling and storage, leading to the continuous accumulation of dead Li and thick surface film formation due to the massive corrosion of Li deposits. The SEI formed on the anodes in the electrolyte containing $LiNO_3$ as a single additive demonstrated the highest O and N contents (Figures S34 and S35), facilitating faster Li-ion transport kinetics. However, this system exhibits the most intensive chemical corrosion and Li-metal losses, suggesting that this faster Li-ion SEI kinetics increases the corrosion rates of the Li deposits and decreases the interphase stability. In contrast, the interphases formed in two electrolytes containing FEC show much less corrosion of Li deposits, thus exhibiting higher stability. This can be attributed to the high F species content that leads to better passivation (very low electron transport, avoiding side reactions between the Li deposits and solution species) and lower Li-ion transport kinetics, which weakens Li deposit corrosion rates (Figures S36 and S37). However, these FEC-containing electrolytes also suffer from capacity loss during aging, despite the smooth surface (Figure 4c), which implies that corrosion occurs in other aspects beyond the surface of the Li-metal deposits, motivating further investigation.

Therefore, electrochemical impedance spectra (EIS) were recorded, accompanied by distribution of relaxation times (DRT) analysis (Figures 4g, S38, and S39). DRT analyzes the impedance in the time domain, enabling differentiation between electrochemical processes with similar time constants that often overlap in Nyquist or Bode plots.[51] Using DRT, we observed distinct trends in the evolution of contact impedance and interphase impedance as a function of the aging time for electrolytes containing FEC or $LiNO_3$ additives (Figure 4h). In the presence of FEC, the contact impedance exhibits a significant increase with aging, reaching over six times its original value, which can be attributed to the contact with the Cu substrate. Conversely, the contact impedance remained relatively stable in the $LiNO_3$-added electrolyte. Regarding the interphase impedance, it shows a more intensive increase upon aging when the interphase was formed in the $LiNO_3$-containing electrolyte compared to the interphase formed in the FEC-containing electrolyte. These results indicate a higher stability of interphases formed on the anodes in the FEC-containing electrolytes.

https://doi.org/10.1021/jacs.4c15759
J. Am. Chem. Soc. 2025, 147, 9365−9377

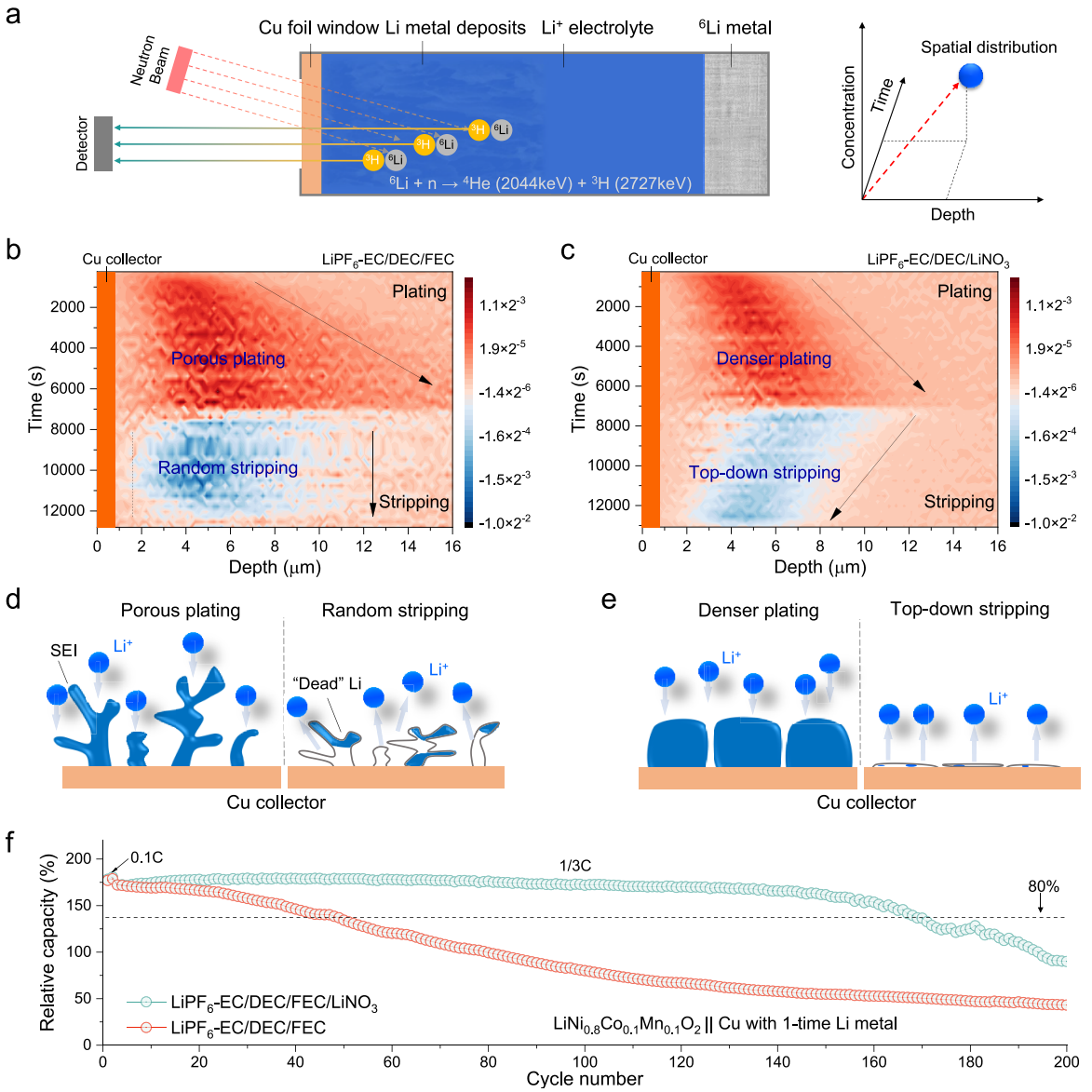

Figure 5. Spatial distribution of Li upon plating/stripping processes. (a) Principle and setup of operando NDP for measuring Li spatial distribution. By capturing the energy loss of the charged ^{3}H (2727 keV), the Li density can be determined as a function of depth and time. (b, c) Li plating/stripping activity from the Li density change. The depth is measured from the Cu current collector, and the color scale indicates Li concentration. (d, e) Schematic illustration of the Li-metal plating/stripping spatial distribution for the electrolytes used based on the observations in (b) and (c), respectively. (d) Electrolytes that show porous Li-metal plating and random stripping. (e) Electrolytes that show denser Li-metal plating and top-down stripping. (f) Cycling performance of NCM811||Cu cells containing the two electrolytes as indicated. The areal capacity of the NCM811 cathode is 2.5 mAh cm^{-2}. An initial amount of Li on the Cu anodes at a same charge density of 2.5 mAh cm^{-2} was predeposited (see explanation in the text) before cycling the NCM811||Cu cells. Cells were operated at a 0.1C rate for the first three cycles and then at a 1/3C rate for the following cycles.

Based on these observations, the corrosion behavior can be qualitatively categorized into different quadrants by mapping the amount of induced dead Li metal versus Li loss by chemical corrosion, as shown in Figure 4i. The interphase formed in the electrolyte with a single FEC additive does not avoid Li-metal corrosion near the Cu current collectors in the cells, inducing the formation of dead Li deposits. Conversely, the interphase formed in the electrolyte containing $LiNO_3$ as a single additive does not avoid losses of active Li metal through intensive corrosion that naturally forms more Li-containing surface species. The interphase formed in the baseline electrolyte shows the least susceptibility of the active Li metal to corrosion during aging, likely due to the presence of thick surface films on the active Li surfaces. These thick surface films reflect a poor passivation capability of the surface species formed by the reactions of the baseline electrolytes with active Li metal. However, thanks to their thickness, the Li surface beneath them reaches passivation (i.e., they succeed in isolating the active Li metal from continuous reactions with the electrolyte). The thick surface films obviously induce nonuniform Li-ion transport through them, naturally stimulating dendritic Li deposition, which necessarily leads to low average CE of the cells containing the baseline electrolyte. By balancing all aspects, the interphases formed in the $LiPF_6$-EC/

https://doi.org/10.1021/jacs.4c15759
J. Am. Chem. Soc. 2025, 147, 9365−9377

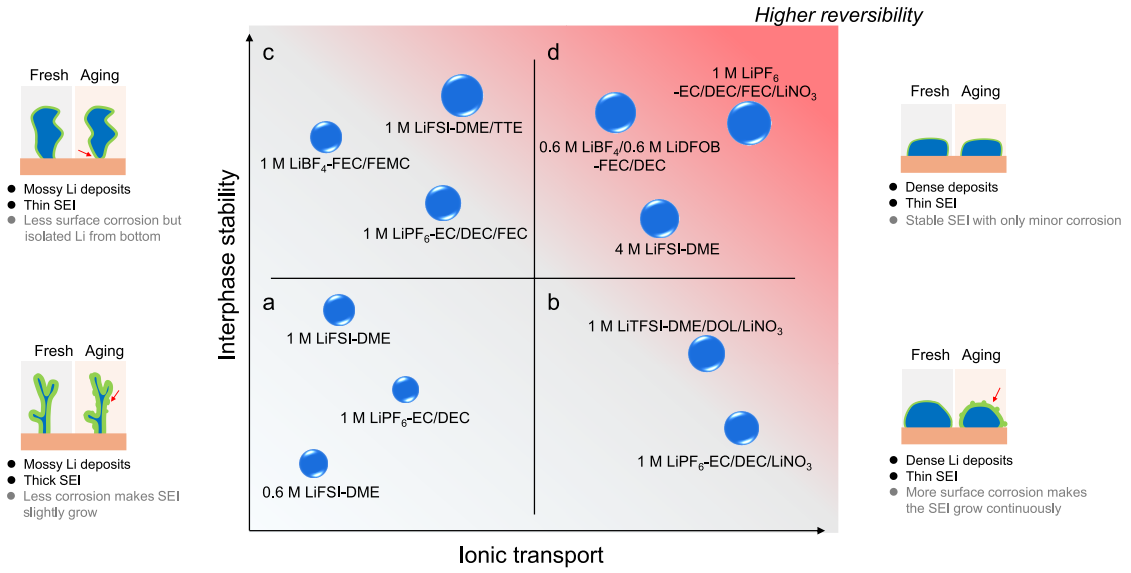

Figure 6. Schematic correlation between the interphase stability and ionic transport. (a) Cases where the properties of the electrolyte dictate the formation of mossy Li deposits and thick SEI; a limited corrosion due to the thick SEI induces only a slight increase in the SEI during aging. (b) Cases where the properties of the electrolyte dictate the formation of dense Li deposits and a relatively thin SEI; during aging, severe corrosion leads to a strong increase in SEI species. (c) Cases where the electrolyte properties dictate the formation of mossy Li deposits and a thin SEI; during aging, intensive corrosion close to the current collector, at the roots of the deposits, leads to dead Li-metal formation upon aging, which potentially can be recovered during subsequent cycling. (d) Cases where the properties of the electrolyte result in the formation of dense Li deposits and a thin SEI; during aging, the Li corrosion is limited, and the SEI is relatively stable suppressing dead Li-metal formation. The size of the colored dots represents the average CE of the cells; the red arrows show the corrosion spots.

DEC/FEC/$LiNO_3$ electrolyte solutions effectively prevent corrosion near the Cu current collectors and minimize the loss of active Li metal due to extensive corrosion. This leads to an overall improvement in the stability of the interphases that passivate Li anodes for rechargeable high-energy-density batteries.

Spatial Distribution of Li during Plating/Stripping Processes. In both continuous cycling and aging, the CE is also influenced by the formation of dead Li, which is observed in the interphases formed in all electrolytes. The evolution, spatial distribution, and relation of dead Li deposits to the interphase properties are very important but poorly understood due to the difficulty in their monitoring, particularly during cell operation. The high selectivity and penetration of neutrons enable noninvasive operando neutron depth profiling (NDP) to explore the spatial distribution of Li. This technique is based on the capture reaction of thermal neutrons of ^{6}Li, producing charged species with a well-defined starting energy (Figure 5a). Measurements of their energy loss allow us to reconstruct the Li density as a function of depth with a time resolution over minutes, providing direct visualization of Li-ion transport behavior and their spatial distribution.[52,53]

During the plating process, Li-metal deposition in the electrolyte containing FEC as a single additive extends to a depth of 16 μm with a scattered distribution into the electrolyte. For the baseline electrolyte, a thicker and more porous Li-metal deposition is observed. In contrast, the electrolytes containing $LiNO_3$ exhibited thinner (~13 μm) and denser Li deposition in them. These findings align well with ex situ SEM analysis (Figure 1). In the electrolyte containing FEC as a single additive, the Li density profiles show asymmetry between plating and stripping (Figure 5b), and the stripping occurs throughout the thickness of the deposits, resulting in porous Li-metal frameworks and the formation of high-surface-area, disconnected Li-metal residues.[15] Conversely, the stripping behavior of deposited Li in the electrolyte containing $LiNO_3$ as a single additive is symmetric (Figure 5c), where the gradually decreasing thickness during Li stripping in this system suggests that stripping initiates from the top of the deposits, indicating a more reversible mechanism.

Figure 5d,e provides a schematic illustration of the spatial distribution of Li-metal plating and stripping, which can be rationalized as follows. The NMR-CEST results indicate that the SEI formed in $LiNO_3$-added electrolytes exhibited better Li-ion transport. This accounts for the denser Li-metal deposits observed in operando NDP (Figures 5c and S40) and SEM (Figure 1c). In contrast, the baseline electrolyte and single FEC-added electrolyte exhibited more porous Li-metal/SEI morphologies. The compact Li-metal deposition in $LiNO_3$-added electrolytes enables more efficient electron transport from the surface of the deposits to the Cu collector, facilitating top-down stripping. Conversely, the more porous deposition compromises the electron transport, resulting in more random stripping. These principles also appear to apply to aging by storage at an open-circuit potential. In that case, chemical corrosion promotes the formation of isolated regions within porous Li-metal deposits, hindering Li-ion transport and lowering reversibility, particularly evident in single FEC-added electrolytes. On the other hand, the single $LiNO_3$-

https://doi.org/10.1021/jacs.4c15759
J. Am. Chem. Soc. 2025, 147, 9365−9377

added electrolyte displays the desired Li plating/stripping behavior. However, its poor interphase stability results in severe chemical corrosion of Li deposits and a consequent irreversible loss of active Li metal, leading to poor cycling efficiency.

Overall, the advantage of using carbonate-based electrolytes in cells with Li-metal anodes and high-voltage cathode materials could enable their application in high-energy-density LMBs. In our proof-of-concept study, we successfully demonstrated the long-term cycling of $LiNi_{0.8}Co_{0.1}Mn_{0.1}O_2$ (NCM811)||Cu cells with a limited content of Li metal (Figures 5f and S41). The cells using 1.0 M $LiPF_6$-EC/DEC/FEC or $LiPF_6$-DE/DEC/FEC/$LiNO_3$ were cycled in the voltage range of 2.8−4.3 V vs Li/Li^+ with NCM811 cathodes' areal capacity of 2.5 mAh cm^{-2}. An initial amount of Li on the Cu anodes at the same charge density of 2.5 mAh cm^{-2} was predeposited. This predeposition of Li was carried out in Li|| Cu cells using the same electrolytes. Then, the Cu anodes with the predeposited Li were transferred to the full cells for cycling. The combination of the FEC and $LiNO_3$ additives results in the best cycling stability of the NCM811||Cu cells and significantly improved capacity retention compared to cells that contained the baseline electrolyte with only FEC as a single additive. This indicates the substantial improvement in the performance of high-energy-density rechargeable Li (metal) batteries that can be achieved via judicious modifications of the interphases formed on the electrodes through the surface chemistry induced by the electrolytes used. We emphasized herein the use of advantageous carbonate solvent-based electrolytes, presenting an effective approach for enhancing LMB performance, through the use of active additives that determine the interfacial surface chemistry in the cells.

Comprehensive Picture of the Correlation between Interphase Stability and Ionic Transport for Li-Metal Anodes. The most important phenomenon in all kinds of Li batteries is that the highly reactive electrodes' interfaces are becoming covered by surface films behaving like SEIs that formed naturally through unavoidable side reactions. These SEIs passivate the active electrodes because they comprise electronically insulting species. However, because they are also composed of ionic Li compounds, they allow Li-ion transport through them. The crucial role of the SEI in Li batteries lies in bridging electrodes and electrolytes, impacting the battery performance. However, due to the complexity and absence of reliable characterization techniques, comprehensively understanding SEI properties remains challenging. To provide a comprehensive understanding of the correlation between interphase stability and ionic transport for Li-metal anodes, we further explored the SEI properties in several state-of-the-art electrolytes. We explored electrolyte systems based on alkyl carbonate solvents because of several well-known advantages of them. Despite their high reactivity toward Li metal anodes, it is possible to manipulate their surface chemistry on Li-metal interfaces through the use of reactive additives in electrolytes. We focused on the impact of the interphase stability and their Li-ion transport capability upon cycling/aging processes, clarifying their intricate relationship, which is summarized in Figure 6. The results of the work described herein showed that it is possible to compose electrolytes that promote the formation of highly Li-ion conducting interphases, resulting in denser Li-metal deposits and favorable top-down stripping, which largely prevents dead Li-metal formation (Figure 6b). However, some interphases of this kind may suffer from severe electrochemical/chemical corrosion, leading to increased impedance upon cycling/aging and irreversible chemical reactions that shorten the Li battery cycle life. On the other hand, electrolytes forming a stable interphase (Figure 6c) can suppress corrosion and minimize active Li-metal loss. The downside of these components is their high barrier for Li-ion diffusion, leading to porous Li-metal deposits and random stripping, causing dead Li formation. Notably, in this case, dead Li metal can be partially reactivated if the SEI layer is not too thick (Figure 6c,d). On the contrary, electrolytes with high-stability salts (e.g., $LiPF_6$) but low-stability solvents (e.g., carbonates) or the low concentration of the salt (as presented in Figure 6a) promote the formation of a thick SEI, posing a larger barrier for Li-ion diffusion between the electrolyte and the Li-metal anode due to the solvent-driven organic-rich interphase components. Although the advantage of the thick SEI is the suppression of corrosion during storage and aging, the disadvantage is the formation of porous and whisker-like Li-metal deposits and random stripping, thereby hindering Li-metal stripping, leading to continuous SEI and dead Li-metal accumulation, resulting in a low average cycling efficiency. Therefore, rational tailoring of electrolytes' chemistries through the judicious selection of their components can enhance interphase ion transport and stability, leading to denser Li-metal deposits and reduced electrochemical/chemical corrosion, as well as improved cycling stability (Figure 6d). A good example is $LiPF_6$-EC/DEC/FEC/$LiNO_3$ electrolytes, which were thoroughly described and discussed herein. Additionally, to further improve the performance of rechargeable Li batteries, factors beyond electrolytes (e.g., substrate, separators, pressure) should be considered to minimize dead Li-metal formation caused by electrochemical/chemical corrosion.

CONCLUSIONS

In summary, with the aim of developing cost-effective electrolytes for LMBs, our study explores the relationship between interphase stability and ionic transport on Li-metal anodes. The comprehensive suite of characterizations, including operando/in situ solid-state NMR spectroscopy, operando NDP, cryo-TEM, and various electrochemical test protocols, allows us to examine interphase properties at different relevant length scales based on the representative electrolyte systems. (1) The small concentration of the additives in solutions we used demonstrated minimal changes in the solvation structures, as was clearly shown by NMR and Raman spectroscopy; however, their presence in solution leads to distinct Li-metal morphologies that do not appear to align with the cycling efficiency of the Li electrodes. This necessitates a re-evaluation of the common belief that the larger the Li deposit size, the more stable cycling can be achieved. (2) The quantification of Li-metal deposits, including active and dead Li metal, and SEI species, was conducted using operando NMR. The SEI structure was further studied using cryo-TEM, showing that the presence of FEC in solutions promotes the formation of a thinner SEI with more inorganic components, consuming less Li. However, it also induces the formation of mossy/dendritic Li-metal deposits and, consequently, dead Li-metal deposits. In contrast, the presence of $LiNO_3$ in solutions results in a slightly thicker and more amorphous SEI, consuming more Li and leading to a lower CE upon long cycling; however, it facilitates larger Li-

https://doi.org/10.1021/jacs.4c15759
J. Am. Chem. Soc. 2025, 147, 9365−9377

metal deposits and reduces the amount of dead Li-metal deposits upon charging. Interestingly, combining both additives does not result in a larger Li deposit size; however, it minimizes Li loss to the SEI and inactive Li metal, leading to higher cycling efficiency. (3) The typically elusive Li-ion transport kinetics across the SEI are directly probed by CEST-NMR measurements, demonstrating that oppositely to FEC, $LiNO_3$ promotes Li-ion transport through the SEI. The effective Li-ion transport facilitates the formation of denser Li-metal deposits because the Li deposition process is faster than the corrosion of the fresh Li deposits by side reactions in solutions. (4) The thermodynamic stability of the Li-metal deposits is examined through an intermittent electrochemical test protocol by introducing an aging step, where three aging mechanisms are observed. A fast Li-ion transport seems to promote direct Li-metal losses toward unrecoverable Li-SEI species, whereas the growth of mossy Li-metal deposits results in the formation of dead Li metal during aging, which can be recovered during subsequent cycling. In contrast, the reference carbonate-based electrolyte solution without additives demonstrates less loss of deposited Li, likely due to the thick SEI formed on Li electrodes in the reference solution. (5) The evolution of the deposited lithium density during the Li metal anodes' charging processes was monitored using operando NDP, revealing that compact Li plating leads to top-down stripping, effectively suppressing the formation of dead Li metal. In contrast, the random Li stripping process occurring with porous Li deposits contributes to the formation of more dead Li metal. Altogether, by directly detecting ion transport across the interphases, we gain insights into how the interphases' chemistry and structure influence the Li plating/stripping behavior. Furthermore, our investigation of interphase stability as a function of the solution compositions revealed the underlying causes of capacity loss during electrochemical cycling, providing valuable guidelines for enhancing cycling performance. Finally, understanding the nature and properties of the interphases formed on Li metal electrodes and correlating it to the level of reversibility exhibited by the Li-metal anodes provide general guidelines for tuning their compositions toward optimal performance.

■ ASSOCIATED CONTENT

Supporting Information

The Supporting Information is available free of charge at https://pubs.acs.org/doi/10.1021/jacs.4c15759.

Detailed materials; experimental procedures; characterization methods; supporting notes and figures, including electrochemical performance, EIS, NMR, and XPS characterizations, as well as properties of electrolytes (PDF)

■ AUTHOR INFORMATION

Corresponding Authors

Qidi Wang − *Department of Radiation Science and Technology, Delft University of Technology, Delft 2629JB, The Netherlands;* orcid.org/0009-0003-3338-0855; Email: q.wang-11@tudelft.nl

Michel Armand − *Centre for Cooperative Research on Alternative Energies (CIC energiGUNE), Basque Research and Technology Alliance (BRTA), 01510 Vitoria-Gasteiz, Spain;* orcid.org/0000-0002-1303-9233; Email: marmand@cicenergigune.com

Doron Aurbach − *Chemistry Department, BINA-BIU Center for Nanotechnology and Advanced Materials and INIES−Israel National Institute for Energy Storage, Bar-Ilan University, Ramat Gan 5290002, Israel;* orcid.org/0000-0001-8047-9020; Email: doron.aurbach@biu.ac.il

Marnix Wagemaker − *Department of Radiation Science and Technology, Delft University of Technology, Delft 2629JB, The Netherlands;* orcid.org/0000-0003-3851-1044; Email: m.wagemaker@tudelft.nl

Authors

Chenglong Zhao − *Department of Radiation Science and Technology, Delft University of Technology, Delft 2629JB, The Netherlands;* orcid.org/0000-0003-0286-8156

Shuwei Wang − *Shenzhen Key Laboratory on Power Battery Safety and Shenzhen Geim Graphene Center, School of Shenzhen International Graduate, Tsinghua University, Beijing, Guangdong 518055, China*

Jianlin Wang − *State Key Laboratory for Surface Physics, Institute of Physics, Chinese Academy of Sciences, Beijing 100190, China;* orcid.org/0000-0002-1749-4428

Fangting Wu − *Shenzhen Key Laboratory on Power Battery Safety and Shenzhen Geim Graphene Center, School of Shenzhen International Graduate, Tsinghua University, Beijing, Guangdong 518055, China*

Pierfrancesco Ombrini − *Department of Radiation Science and Technology, Delft University of Technology, Delft 2629JB, The Netherlands*

Swapna Ganapathy − *Department of Radiation Science and Technology, Delft University of Technology, Delft 2629JB, The Netherlands;* orcid.org/0000-0001-5265-1663

Stephen Eustace − *Department of Biotechnology, Delft University of Technology, Delft 2629HZ, The Netherlands*

Xuedong Bai − *State Key Laboratory for Surface Physics, Institute of Physics, Chinese Academy of Sciences, Beijing 100190, China;* orcid.org/0000-0002-1403-491X

Baohua Li − *Shenzhen Key Laboratory on Power Battery Safety and Shenzhen Geim Graphene Center, School of Shenzhen International Graduate, Tsinghua University, Beijing, Guangdong 518055, China*

Complete contact information is available at: https://pubs.acs.org/10.1021/jacs.4c15759

Author Contributions

$^{\nabla}$Q.W., C.Z., and S.W. contributed equally to this work.

Notes

The authors declare no competing financial interest.

■ ACKNOWLEDGMENTS

This work was supported by Netherlands Organization for Scientific Research (NWO) under VICI (No. 16122) and Shell Global Solutions International B.V., the National Natural Science Foundation of China (Grant No. 52302249), Chinese Academy of Sciences (Grant No. XDB33000000), Special Fund Project for Strategic Emerging Industry Development of Shenzhen (No. 20170428145209110), and Local Innovative and Research Teams Project of Guangdong Pearl River Talents Program (No. 2017BT01N111).

■ REFERENCES

(1) Tarascon, J. M.; Armand, M. Issues and challenges facing rechargeable lithium batteries. *Nature* **2001**, *414* (6861), 359−367.

(2) Whittingham, M. Stanley, Lithium Batteries and Cathode Materials. *Chem. Rev.* **2004**, *104* (10), 4271−4302.
(3) Cheng, X.B.; Zhang, R.; Zhao, C.Z.; Zhang, Q. Toward Safe Lithium Metal Anode in Rechargeable Batteries: A Review. *Chem. Rev.* **2017**, *117* (15), 10403−10473.
(4) Wang, Q.; Yao, Z.; Wang, J.; Guo, H.; Li, C.; Zhou, D.; Bai, X.; Li, H.; Li, B.; Wagemaker, M.; Zhao, C. Chemical short-range disorder in lithium oxide cathodes. *Nature* **2024**, *629* (8011), 341−347.
(5) Lin, D.; Liu, Y.; Cui, Y. Reviving the lithium metal anode for high-energy batteries. *Nat. Nanotechnol.* **2017**, *12* (3), 194−206.
(6) Yamada, Y.; Yamada, A. Superconcentrated Electrolytes for Lithium Batteries. *J. Electrochem. Soc.* **2015**, *162*, A2406−A2423.
(7) Wang, H.; Yu, Z.; Kong, X.; Kim, S.C.; Boyle, D.T.; Qin, J.; Bao, Z.; Cui, Y. Liquid electrolyte: The nexus of practical lithium metal batteries. *Joule* **2022**, *6* (3), 588−616.
(8) Xu, K. Electrolytes and Interphases in Li-Ion Batteries and Beyond. *Chem. Rev.* **2014**, *114* (23), 11503−11618.
(9) Aurbach, D.; Zaban, A.; Schechter, A.; Ein-Eli, Y.; Zinigrad, E.; Markovsky, B. The Study of Electrolyte Solutions Based on Ethylene and Diethyl Carbonates for Rechargeable Li Batteries: I. Li Metal Anodes. *J. Electrochem. Soc.* **1995**, *142* (9), 2873.
(10) Ding, F.; Xu, W.; Chen, X.; Zhang, J.; Engelhard, M.H.; Zhang, Y.; Johnson, B.R.; Crum, J.V.; Blake, T.A.; Liu, X.; Zhang, J.G. Effects of Carbonate Solvents and Lithium Salts on Morphology and Coulombic Efficiency of Lithium Electrode. *J. Electrochem. Soc.* **2013**, *160* (10), A1894.
(11) Mogi, R.; Inaba, M.; Jeong, S.K.; Iriyama, Y.; Abe, T.; Ogumi, Z. Effects of Some Organic Additives on Lithium Deposition in Propylene Carbonate. *J. Electrochem. Soc.* **2002**, *149* (12), A1578.
(12) Wang, Q.; Zhao, C.; Wang, S.; Wang, J.; Liu, M.; Ganapathy, S.; Bai, X.; Li, B.; Wagemaker, M. Clarifying the Relationship between the Lithium Deposition Coverage and Microstructure in Lithium Metal Batteries. *J. Am. Chem. Soc.* **2022**, *144* (48), 21961−21971.
(13) Wang, Q.; Zhao, C.; Yao, Z.; Wang, J.; Wu, F.; Kumar, S.G.H.; Ganapathy, S.; Eustace, S.; Bai, X.; Li, B.; Lu, J.; Wagemaker, M. Entropy-Driven Liquid Electrolytes for Lithium Batteries. *Adv. Mater.* **2023**, *35* (17), No. 2210677.
(14) Louli, A.J.; Eldesoky, A.; Weber, R.; Genovese, M.; Coon, M.; deGooyer, J.; Deng, Z.; White, R.T.; Lee, J.; Rodgers, T.; Petibon, R.; Hy, S.; Cheng, S.J.H.; Dahn, J.R. Diagnosing and correcting anode-free cell failure via electrolyte and morphological analysis. *Nat. Energy* **2020**, *5* (9), 693−702.
(15) Wang, Q.; Yao, Z.; Zhao, C.; Verhallen, T.; Tabor, D.P.; Liu, M.; Ooms, F.; Kang, F.; Aspuru-Guzik, A.; Hu, Y.S.; Wagemaker, M.; Li, B. Interface chemistry of an amide electrolyte for highly reversible lithium metal batteries. *Nat. Commun.* **2020**, *11* (1), 4188.
(16) Fan, X.; Chen, L.; Borodin, O.; Ji, X.; Chen, J.; Hou, S.; Deng, T.; Zheng, J.; Yang, C.; Liou, S.C.; Amine, K.; Xu, K.; Wang, C. Non-flammable electrolyte enables Li-metal batteries with aggressive cathode chemistries. *Nat. Nanotechnol.* **2018**, *13* (8), 715−722.
(17) Yu, Z.; Rudnicki, P.E.; Zhang, Z.; Huang, Z.; Celik, H.; Oyakhire, S.T.; Chen, Y.; Kong, X.; Kim, S.C.; Xiao, X.; Wang, H.; Zheng, Y.; Kamat, G.A.; Kim, M.S.; Bent, S.F.; Qin, J.; Cui, Y.; Bao, Z. Rational solvent molecule tuning for high-performance lithium metal battery electrolytes. *Nat. Energy* **2022**, *7* (1), 94−106.
(18) Chen, S.; Zheng, J.; Yu, L.; Ren, X.; Engelhard, M.H.; Niu, C.; Lee, H.; Xu, W.; Xiao, J.; Liu, J.; Zhang, J.G. High-Efficiency Lithium Metal Batteries with Fire-Retardant Electrolytes. *Joule* **2018**, *2* (8), 1548−1558.
(19) Piao, N.; Ji, X.; Xu, H.; Fan, X.; Chen, L.; Liu, S.; Garaga, M.N.; Greenbaum, S.G.; Wang, L.; Wang, C.; He, X. Countersolvent Electrolytes for Lithium-Metal Batteries. *Adv. Energy Mater.* **2020**, *10* (10), No. 1903568.
(20) Cao, X.; Jia, H.; Xu, W.; Zhang, J.G. Review—Localized High-Concentration Electrolytes for Lithium Batteries. *J. Electrochem. Soc.* **2021**, *168* (1), No. 010522.
(21) Ren, X.; Zou, L.; Cao, X.; Engelhard, M.H.; Liu, W.; Burton, S.D.; Lee, H.; Niu, C.; Matthews, B.E.; Zhu, Z.; Wang, C.; Arey, B.W.; Xiao, J.; Liu, J.; Zhang, J.G.; Xu, W. Enabling High-Voltage Lithium-Metal Batteries under Practical Conditions. *Joule* **2019**, *3* (7), 1662−1676.
(22) Zhang, X.; Cheng, X.; Chen, X.; Yan, C.; Zhang, Q. Fluoroethylene Carbonate Additives to Render Uniform Li Deposits in Lithium Metal Batteries. *Adv. Funct. Mater.* **2017**, *27* (10), No. 1605989.
(23) Shkrob, I.A.; Wishart, J.F.; Abraham, D.P. What Makes Fluoroethylene Carbonate Different? *J. Phys. Chem. C* **2015**, *119* (27), 14954−14964.
(24) Zhao, Q.; Stalin, S.; Archer, L.A. Stabilizing metal battery anodes through the design of solid electrolyte interphases. *Joule* **2021**, *5* (5), 1119−1142.
(25) Aurbach, D.; Ein-Ely, Y.; Zaban, A. The Surface Chemistry of Lithium Electrodes in Alkyl Carbonate Solutions. *J. Electrochem. Soc.* **1994**, *141* (1), L1.
(26) Yang, Q.; Hu, J.; Meng, J.; Li, C. C−F-rich oil drop as a non-expendable fluid interface modifier with low surface energy to stabilize a Li metal anode. *Energy Environ. Sci.* **2021**, *14* (6), 3621−3631.
(27) Yu, Y.; Lai, C.; Lei, M.; Chen, K.; Li, C. Dual strategies of mild C−F scissoring fluorination and local high-concentration electrolyte to enable reversible Li−Fe−F conversion batteries. *Mater. Horizons* **2024**, *11* (9), 2169−2179.
(28) Liu, Y.; Lin, D.; Li, Y.; Chen, G.; Pei, A.; Nix, O.; Li, Y.; Cui, Y. Solubility-mediated sustained release enabling nitrate additive in carbonate electrolytes for stable lithium metal anode. *Nat. Commun.* **2018**, *9* (1), 3656.
(29) Suo, L.; Borodin, O.; Gao, T.; Olguin, M.; Ho, J.; Fan, X.; Luo, C.; Wang, C.; Xu, K. Water-in-salt" electrolyte enables high-voltage aqueous lithium-ion chemistries. *Science* **2015**, *350* (6263), 938−943.
(30) Wang, C.; Meng, Y.S.; Xu, K. Perspective—Fluorinating Interphases. *J. Electrochem. Soc.* **2019**, *166* (3), A5184.
(31) Yao, Y.; Chen, X.; Yan, C.; Zhang, X.; Cai, W.; Huang, J.; Zhang, Q. Regulating Interfacial Chemistry in Lithium-Ion Batteries by a Weakly Solvating Electrolyte. *Angew. Chem., Int. Ed.* **2021**, *60* (8), 4090−4097.
(32) Kim, M.S.; Zhang, Z.; Rudnicki, P.E.; Yu, Z.; Wang, J.; Wang, H.; Oyakhire, S.T.; Chen, Y.; Kim, S.C.; Zhang, W.; Boyle, D.T.; Kong, X.; Xu, R.; Huang, Z.; Huang, W.; Bent, S.F.; Wang, L.W.; Qin, J.; Bao, Z.; Cui, Y. Suspension electrolyte with modified^{+} solvation environment for lithium metal batteries. *Nat. Mater.* **2022**, *21* (4), 445−454.
(33) Yu, Z.; Wang, H.; Kong, X.; Huang, W.; Tsao, Y.; Mackanic, D.G.; Wang, K.; Wang, X.; Huang, W.; Choudhury, S.; Zheng, Y.; Amanchukwu, C.V.; Hung, S.T.; Ma, Y.; Lomeli, E.G.; Qin, J.; Cui, Y.; Bao, Z. Molecular design for electrolyte solvents enabling energy-dense and long-cycling lithium metal batteries. *Nat. Energy* **2020**, *5* (7), 526−533.
(34) Boyle, D.T.; Kim, S.C.; Oyakhire, S.T.; Vilá, R.A.; Huang, Z.; Sayavong, P.; Qin, J.; Bao, Z.; Cui, Y. Correlating Kinetics to Cyclability Reveals Thermodynamic Origin of Lithium Anode Morphology in Liquid Electrolytes. *J. Am. Chem. Soc.* **2022**, *144* (45), 20717−20725.
(35) Meng, J.; Lei, M.; Lai, C.; Wu, Q.; Liu, Y.; Li, C. Lithium Ion Repulsion-Enrichment Synergism Induced by Core−Shell Ionic Complexes to Enable High-Loading Lithium Metal Batteries. *Angew. Chem., Int. Ed.* **2021**, *60* (43), 23256−23266.
(36) Bhattacharyya, R.; Key, B.; Chen, H.; Best, A.S.; Hollenkamp, A.F.; Grey, C.P. In situ NMR observation of the formation of metallic lithium microstructures in lithium batteries. *Nat. Mater.* **2010**, *9* (6), 504−510.
(37) Pecher, O.; Bayley, P.M.; Liu, H.; Liu, Z.; Trease, N.M.; Grey, C.P. Automatic Tuning Matching Cycler (ATMC) in situ NMR spectroscopy as a novel approach for real-time investigations of Li- and Na-ion batteries. *J. Magn. Reson.* **2016**, *265*, 200−209.
(38) May, R.; Fritzsching, K.J.; Livitz, D.; Denny, S.R.; Marbella, L.E. Rapid Interfacial Exchange of Li Ions Dictates High Coulombic Efficiency in Li Metal Anodes. *ACS Energy Lett.* **2021**, *6* (4), 1162−1169.

https://doi.org/10.1021/jacs.4c15759
J. Am. Chem. Soc. 2025, 147, 9365−9377

(39) Gunnarsdóttir, A.B.; Vema, S.; Menkin, S.; Marbella, L.E.; Grey, C.P. Investigating the effect of a fluoroethylene carbonate additive on lithium deposition and the solid electrolyte interphase in lithium metal batteries using in situ NMR spectroscopy. *J. Mater. Chem. A* **2020**, *8* (30), 14975−14992.
(40) Columbus, D.; Arunachalam, V.; Glang, F.; Avram, L.; Haber, S.; Zohar, A.; Zaiss, M.; Leskes, M. Direct Detection of Lithium Exchange across the Solid Electrolyte Interphase by 7Li Chemical Exchange Saturation Transfer. *J. Am. Chem. Soc.* **2022**, *144* (22), 9836−9844.
(41) Vinogradov, E.; Sherry, A.D.; Lenkinski, R.E. CEST: From basic principles to applications, challenges and opportunities. *J. Magn. Reson.* **2013**, *229*, 155−172.
(42) Ward, K. M.; Aletras, A. H.; Balaban, R. S. A New Class of Contrast Agents for MRI Based on Proton Chemical Exchange Dependent Saturation Transfer (CEST). *J. Magn. Reson.* **2000**, *143* (1), 79−87.
(43) Wang, Q.; Zhao, C.; Hu, X.; Wang, J.; Ganapathy, S.; Eustace, S.; Bai, X.; Li, B.; Li, H.; Aurbach, D.; Wagemaker, M. Grain-Boundary-Rich Interphases for Rechargeable Batteries. *J. Am. Chem. Soc.* **2024**, *146* (46), 31778−31787.
(44) Guivel-Scharen, V.; Sinnwell, T.; Wolff, S. D.; Balaban, R. S. Detection of Proton Chemical Exchange between Metabolites and Water in Biological Tissues. *J. Magn. Reson.* **1998**, *133* (1), 36−45.
(45) McConnell, H.M. Reaction Rates by Nuclear Magnetic Resonance. *J. Chem. Phys.* **1958**, *28* (3), 430−431.
(46) Woessner, D.E.; Zhang, S.; Merritt, M.E.; Sherry, A.D. Numerical solution of the Bloch equations provides insights into the optimum design of PARACEST agents for MRI. *Magn. Reson. Med.* **2005**, *53* (4), 790−799.
(47) Zaiss, M.; Bachert, P. Exchange-dependent relaxation in the rotating frame for slow and intermediate exchange−modeling off-resonant spin-lock and chemical exchange saturation transfer. *NMR Biomed.* **2013**, *26* (5), 507−518.
(48) Dubarry, M.; Qin, N.; Brooker, P. Calendar aging of commercial Li-ion cells of different chemistries−A review. *Curr. Opin. Electrochem.* **2018**, *9*, 106−113.
(49) Keil, P.; Schuster, S.F.; Wilhelm, J.; Travi, J.; Hauser, A.; Karl, R.C.; Jossen, A. Calendar Aging of Lithium-Ion Batteries. *J. Electrochem. Soc.* **2016**, *163* (9), A1872.
(50) Boyle, D.T.; Huang, W.; Wang, H.; Li, Y.; Chen, H.; Yu, Z.; Zhang, W.; Bao, Z.; Cui, Y. Corrosion of lithium metal anodes during calendar ageing and its microscopic origins. *Nat. Energy* **2021**, *6* (5), 487−494.
(51) Chang, H.J.; Trease, N.M.; Ilott, A.J.; Zeng, D.; Du, L.S.; Jerschow, A.; Grey, C.P. Investigating Li microstructure formation on Li anodes for lithium batteries by in situ ^{6}Li/^{7}Li NMR and SEM. *J. Phys. Chem. C* **2015**, *119* (29), 16443−16451.
(52) Verhallen, T. W.; Lv, S.; Wagemaker, M. Operando Neutron Depth Profiling to Determine the Spatial Distribution of Li in Li-ion Batteries. *Front. Energy Res.* **2018**, *6*, 62.
(53) Lv, S.; Verhallen, T.; Vasileiadis, A.; Ooms, F.; Xu, Y.; Li, Z.; Li, Z.; Wagemaker, M. Operando monitoring the lithium spatial distribution of lithium metal anodes. *Nat. Commun.* **2018**, *9* (1), 2152.
(54) Gunnarsdóttir, A.B.; Amanchukwu, C.V.; Menkin, S.; Grey, C.P. Noninvasive In Situ NMR Study of "Dead Lithium" Formation and Lithium Corrosion in Full-Cell Lithium Metal Batteries. *J. Am. Chem. Soc.* **2020**, *142* (49), 20814−20827.

NOTE ADDED AFTER ASAP PUBLICATION

This paper was published ASAP on March 7, 2025. Corrections were made to Figure 2, and the corrected version was reposted on March 10, 2025.

https://doi.org/10.1021/jacs.4c15759
J. Am. Chem. Soc. 2025, 147, 9365−9377